

Potential effect of the deformation of strong-coupling polaron in perovskite materials

Jing Bai(白静), Ran An(安然), Xin-Xue Zhang(张新雪), Hui-Yi Cai(蔡蕙翼), Xin-Xin Duan(段欣欣), Xin Zhang(张鑫), Xin-Jun Ma(马新军), Yong Sun(孙勇)

Citation: Chin. Phys. B. 35, 097101 (2026). DOI: 10.1088/1674-1056/ae1c20 |
CSTR: 32038.14.CPB.ae1c20
http://cpb.iphy.ac.cn; http://iopscience.iop.org/cpb

What follows is a list of articles you may be interested in

Suppression of moving-potential effect in an optical Raman lattice scheme for spin–orbit-coupled alkaline-earth fermions

Rui Wu(吴瑞), Han Zhang(张涵), Tao Deng(邓涛), Wen-Wei Wang(王文伟), Xibo Zhang(张熙博)
Chin. Phys. B. 35, 067102 (2026). DOI: 10.1088/1674-1056/ae4c71 | CSTR: 32038.14.CPB.ae4c71

Sequential phase transformations in $Ta_{0.4}Ti_2Zr$ alloy via tensile molecular dynamics simulations with deep potential

Hongyang Liu(刘洪洋), Rong Chen(陈荣), Bo Chen(陈博), Jingzhi He(贺靖之), Dongdong Kang(康冬冬), Jiayu Dai(戴佳钰)
Chin. Phys. B. 35, 017102 (2026). DOI: 10.1088/1674-1056/ae1e68 | CSTR: 32038.14.CPB.ae1e68

Ground state of electron-doped *t*–*t*′–*J* model on cylinders: An investigation of finite size and boundary condition effects

Yang Shen(沈阳), Xiangjian Qian(钱湘坚), Mingpu Qin(秦明普)
Chin. Phys. B. 34, 087105 (2025). DOI: 10.1088/1674-1056/add00b | CSTR: 32038.14.CPB.add00b

Ab initio prediction of ground-state magnetic ordering and high-pressure magnetic phase transition of uranium mononitride

Jing-Jing Zheng(郑晶晶), Yuxi Chen(陈禹西), Chengxiang Zhao(赵承祥), Junfeng Zhang(张均锋), Ping Zhang(张平), Bao-Tian Wang(王保田), Jiang-Jiang Ma(马江将)
Chin. Phys. B. 34, 087101 (2025). DOI: 10.1088/1674-1056/add4e6 | CSTR: 32038.14.CPB.add4e6

First principles investigation of protactinium-based oxide-perovskites for flexible opto—electronic devices

Nazia Erum, Muhammad Azhar Iqbal
Chin. Phys. B. 26, 047102 (2017). DOI: 10.1088/1674-1056/26/4/047102

Potential effect of the deformation of strong-coupling polaron in perovskite materials

Jing Bai(白静)[1,2], Ran An(安然)[1,2], Xin-Xue Zhang(张新雪)[1,2], Hui-Yi Cai(蔡蕙翼)[1,2], Xin-Xin Duan(段欣欣)[1,2], Xin Zhang(张鑫)[1,2], Xin-Jun Ma(马新军)[1,2], and Yong Sun(孙勇)[1,2,†]

[1] *College of Physics and Electronic Information, Inner Mongolia Minzu University, Tongliao* 028000, *China*
[2] *Institute of Condensed Matter Physics, Inner Mongolia Minzu University, Tongliao* 028000, *China*

(Received 2 September 2025; revised manuscript received 30 October 2025; accepted manuscript online 6 November 2025)

The electronic structure of perovskite nanomaterial systems can change when exposed to mechanical stress, a fact that has been extensively applied in the investigation of polaron properties. A deformation potential is formed when interactions among charge carriers and the lattice are mediated by stress. Hence, the deformation potential can be considered an important tool to explore acoustic polaron properties. In this research, we adopted a theoretical method by combining unitary transformation and second quantization, incorporating the deformation potential effect into the polaron effect. Finally, we derived the effective mass and ground-state energy of strongly coupled bound polarons in perovskite lattices. Through in-depth analysis and numerical calculations, we found that under the combined influence of sound velocity and deformation potential, the polaron coupling strength no longer remained constant; instead, it exhibited a variation with the perovskite lattice deformation potential. In addition, the ground-state energy, vibrational frequency, and effective mass of the polaron displayed anomalous behaviors. This research provides an important reference to further understand the physical characteristics of acoustic polarons formed by lattice distortions.

Keywords: deformation potential, ground-state energy, acoustic polaron, effective mass, perovskite

PACS: 71.38.–k, 73.21.Fg, 63.20.kd, 63.22.–m

DOI: 10.1088/1674-1056/ae1c20 **CSTR:** 32038.14.CPB.ae1c20

1. Introduction

In condensed matter physics, the term "polaron" is generally applied to describing a type of Fermi quasiparticle consisting of an excess charge in a material lattice and the accompanying lattice distortion it induces.[1–4] Polarons, as an essential type of quasiparticle, play a key role in understanding the optical and electrical characteristics of materials. This polaron effect is commonly witnessed in organic semiconductors,[5,6] polar crystals,[7,8] ionic crystals,[9,10] and perovskite materials,[11] where the optical phonon modes of lattice vibrations polarize charge carriers via long-range Coulomb interactions (Fröhlich potential). Elastic waves from lattice vibrations affect the charge carriers which interact with phonons, resulting in lattice distortions to generate elastic potential energy around the carriers. When this potential energy is large enough, carriers become trapped in deep potential wells, giving rise to the formation of a bound state, also referred to as deformation potential polaron. Investigation of the nature of deformation potentials in materials plays a key role in understanding their piezoelectric conversion characteristics.[12–14] Investigating the aforementioned polaron effects necessitates a material platform capable of exhibiting significant lattice responses to external fields, such as stress. Perovskite materials emerge as an ideal candidate for such studies due to their inherent soft lattice character, which confers low lattice stiffness and enables pronounced deformation under minimal external force, thereby giving rise to a substantial deformation potential. This unique attribute not only directly enhances the electron–phonon coupling strength but also facilitates the direct manipulation of the polaron state via applied stress, thereby providing a crucial foundation for elucidating the underlying structure-property relationships at the microscopic level.

When exploring the deformation potential effect on polarons, the most essential feature is the electron–phonon interactions within the material. The strength of these interactions, referred to as coupling strength, is determined by the material's dimensionless lattice constant. However, under the deformation potential effect, the material's structural properties exert direct or indirect influences on coupling strength, resulting in unique acoustic polaron effects. That is, quasiparticle effects demonstrate certain differences for different material systems. Through detailed evaluation of the dimensionless lattice constant, deformation potential, and coupling strength of a material, one can better understand and predict electron–phonon interactions. This understanding can provide more targeted guidance for developing and applying related devices.

Several researchers have applied experimental approaches to observe polarons, including microscopic ap-

†Corresponding author. E-mail: sy19851009@126.com

© 2026 Chinese Physical Society and IOP Publishing Ltd. All rights, including for text and data mining, AI training, and similar technologies, are reserved.

proaches such as scanning tunneling microscopy (STM)[15] and spectroscopic methods such as electron paramagnetic resonance (EPR),[16] angle-resolved spectroscopy,[17] Raman spectroscopy,[18] two-photon photoelectron spectroscopy,[19] and high-time-resolution spectroscopy.[20,21] Recently, Tang[22] successfully tracked the process of polaron formation using ultrafast spectroscopic approaches. However, while these experimental research works[23–26] have provided qualitative descriptions of polaron properties, more theoretical studies are still needed to quantitatively analyze polaron-related physical properties.[27–30]

Hence, this research adopted a concise theoretical method combining unitary transformation and second quantization to evaluate unique deformation potential polaron effects. By systematic examination of the ground-state energy, vibrational frequency, and effective mass of the polaron, we obtained fundamental conclusions that provided crucial theoretical support for experimental characterization methods including mobility analyses and spectroscopic measurements.

2. Theoretical model

When electrons move within perovskite materials, considering only one-dimensional (1D) motion where they are affected by deformation potential and interact with acoustic phonons, the Hamiltonian of the system can be stated as

$$H = \frac{p^2}{2m} + \sum_k \hbar s k a_k^\dagger a_k + \left(\frac{4\pi\alpha}{L}\right)^{1/2} \times \sum_k \hbar s k^{1/2} \left(a_k + a_{-k}^\dagger\right) \mathrm{e}^{\mathrm{i}kx}, \tag{1}$$

where a_k and $a_k^\dagger$ are the acoustic phonon annihilation and creation operators, respectively, m is the electron mass, k is the wave vector, p and x are the momentum and position operators of the electron, respectively, and L is the normalization length. In Eq. (1), the term $p^2/2m$ describes the kinetic energy of the electron, and $\sum_k \hbar s|k| a_k^\dagger a_k$ is the deformation potential phonon energy, with s being the sound velocity that varies for different perovskite materials. When pressure is applied along two dimensions, the electron is forced into 1D motion. The electron–phonon interaction energy

$$\left(\frac{4\pi\alpha}{L}\right)^{1/2} \sum_k \hbar s k^{1/2} \left(a_k + a_{-k}^\dagger\right) \mathrm{e}^{\mathrm{i}kx}$$

depends on the sound velocity, the normalized length, the coupling constant, and the wave vector. The coupling strength was given by α as follows:

$$\alpha = \frac{1}{8\pi} \frac{aD^2}{\hbar M s^3}, \tag{2}$$

where a is the lattice constant, D is the deformation potential constant, and M is the charge per unit cell. Therefore, by controlling the deformation potential and lattice constants, the coupling strength could be modulated, which could in turn regulate the electron–phonon interaction energy and ultimately tune the acoustic polaron energy. Figure 1 illustrates the piezoelectric polaron effect under the influence of different deformation potentials, subjected to both compressive and tensile strains.

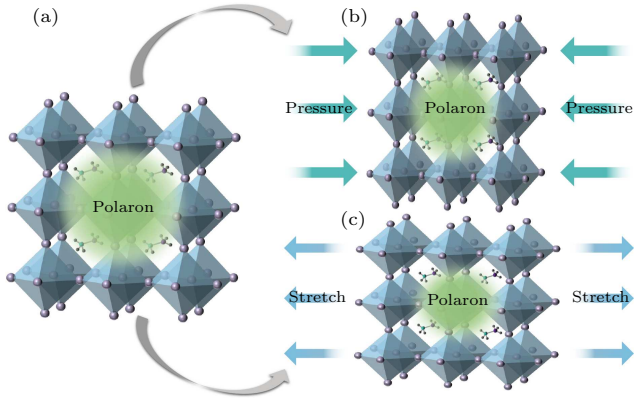


Fig. 1. Piezoelectric polaron effect.

To calculate the ground-state energy and effective mass of the polaron, we considered the total momentum of the system to comprise two components: the momentum of the electron and the momentum of the phonon. Therefore, we introduced the total momentum operator P as

$$P = p + \sum_k \hbar s k a_k^\dagger a_k. \tag{3}$$

To further process the position and momentum operators in the Hamiltonian and achieve its final form, we introduced the annihilation operator b and creation operator $b^\dagger$, using second quantization for both position and momentum coordinates as follows:

$$p = \left(\frac{m\hbar\lambda}{2}\right)^{1/2} \left(b^\dagger + b + p_0\right), \tag{4}$$

$$x = \mathrm{i}\left(\frac{\hbar}{2m\lambda}\right)^{1/2} \left(b - b^\dagger\right), \tag{5}$$

where λ and p_0 are variational parameters. By substituting the second-quantized position and momentum operators into the Hamiltonian in Eq. (1), we obtained

$$H' = \frac{\hbar\lambda}{4}\left(b^\dagger + b + p_0\right)^2 + \sum_k \hbar s|k| a_k^\dagger a_k + \left(\frac{4\pi\alpha}{L}\right)^{1/2} \sum_k \hbar s\sqrt{k}\left(a_k + a_{-k}^\dagger\right) \times \exp\left(\mathrm{i}ki\left(\frac{\hbar}{2m\lambda}\right)^{1/2}\left(b - b^\dagger\right)\right). \tag{6}$$

Performing a unitary transformation on the Hamiltonian H' gave

$$U = \exp\left[\sum_k \left(f_k a_k^\dagger - f_k^* a_k\right)\right]. \tag{7}$$

Performing a unitary transformation yielded the transformed Hamiltonian as

$$\begin{aligned} H'' &= U_2^{-1} H' U_2 \\ &= \frac{\hbar\lambda}{4}\left(b^\dagger + b + p_0\right)^2 + \sum_k \hbar s|k|\left(a_k^\dagger + f_k^*\right)(a_k + f_k) \\ &\quad + \left(\frac{4\pi\alpha}{L}\right)^{1/2} \sum_k \hbar s\sqrt{k}\left(a_k + f_k + a_{-k}^\dagger + f_{-k}^*\right) \\ &\quad \times \exp\left(\mathrm{i}ki\left(\frac{\hbar}{2m\lambda}\right)^{1/2}\left(b - b^\dagger\right)\right). \end{aligned} \tag{8}$$

To determine the effective mass and ground-state energy of the system, we first calculated the partially corrected Hamiltonian as

$$\begin{aligned} u\cdot P &= u\cdot\left(p + \sum_k \hbar s k a_k^\dagger a_k\right) \\ &= u\left(\frac{m\hbar\lambda}{2}\right)^{1/2}\left(b^\dagger + b + p_0\right) + u\sum_k \hbar s k a_k^\dagger a_k. \end{aligned} \tag{9}$$

The final Hamiltonian was derived by the substitution of the partially corrected Hamiltonian into the polaron Hamiltonian. We then performed a unitary transformation on the final Hamiltonian and calculated the energy expectation value as:

$$\begin{aligned} &F(\lambda, f_k, p_0, u) \\ &= \langle 0|U^{-1}(H - u\cdot P)U|0\rangle \\ &= \frac{\hbar\lambda}{4}p_0^2 + \frac{\hbar\lambda}{4} + \sum_k \hbar s|k||f_k|^2 \\ &\quad + \left(\frac{4\pi\alpha}{L}\right)^{1/2}\sum_k \hbar s\sqrt{k}\left(f_k^* + f_k\right)\mathrm{e}^{-\hbar k^2/4m\lambda} \\ &\quad - \sum_k u\hbar s k|f_k|^2 - up_0\sqrt{\left(\frac{m\hbar\lambda}{2}\right)}. \end{aligned} \tag{10}$$

Here, the zero-polaron state $|0\rangle = |0\rangle_{\mathrm{e}}|0\rangle_{\mathrm{p}}$ consisted of the zero-electron state $|0\rangle_{\mathrm{e}}$ and the zero-phonon state $|0\rangle_{\mathrm{p}}$. Then, the expectation value functional F was changed with respect to the variational parameters f_k^*, p_0, and λ,

$$\frac{\partial F}{\partial f_k^*} = 0. \tag{11}$$

We derived the displacement parameter characterizing interactions among electrons moving in the lattice and phonons as

$$f_k = -\frac{\left(\frac{4\pi\alpha}{L}\right)^{1/2}\hbar s\sqrt{k}\,\mathrm{e}^{-\hbar k^2/4m\lambda}}{\hbar s|k| - u\hbar k}. \tag{11a}$$

The expectation value functional F was changed with respect to the initial momentum of the electron p_0 as

$$\frac{\partial F}{\partial p_0} = 0. \tag{12}$$

The initial momentum was derived as

$$p_0 = u\sqrt{\frac{2m}{\hbar\lambda}}, \tag{12a}$$

$$\frac{\partial F}{\partial \lambda} = 0, \tag{13}$$

and the variation frequency was obtained as

$$\lambda = \frac{32\pi\alpha^2 s^6 m}{\hbar\left(s^2 - u^2\right)^2}. \tag{13a}$$

The expressions of f_k^*, p_0, and λ were substituted back into the original Hamiltonian of the polaron to obtain the polaron ground-state energy in the perovskite material as

$$E_0 = \bar{F} = \frac{\hbar\lambda}{4} - \frac{1}{2}mu^2 - \frac{2\alpha s^3\sqrt{2\pi m\lambda\hbar}}{\left(s^2 - u^2\right)}. \tag{14}$$

To derive the effective mass, we performed a unitary transformation on the momentum and applied it to the zero-polaron state as

$$\begin{aligned} \langle 0|U^{-1}PU|\rangle &= \left[-F(\lambda, p_0, u) + \langle 0|U^{-1}HU|\rangle\right]/u \\ &= u\left[m + \frac{32\pi\alpha^2 s^6 m}{\left(s^2 - u^2\right)^3}\right]. \end{aligned} \tag{15}$$

The polaron effective mass was obtained as

$$m^* = m + \frac{32\pi\alpha^2 s^6 m}{\left(s^2 - u^2\right)^3}. \tag{16}$$

From the above equation, we derived the relationship between the bare electron mass and the polaron effective mass, which further allowed us to identify the factors affecting the polaron effective mass.

3. Results and discussion

To explore the ground-state features of strongly coupled bound polarons in deformation potential, numerical calculations were conducted on the following three metal halide perovskite crystals with strong polaron effects: $MAPbCl_3$, $MAPbBr_3$, and $MAPbI_3$. A detailed discussion is provided below on strong coupling interactions among acoustic phonons and electrons, and the relevant material parameters are listed in Table 1.

Table 1. Parameters of different perovskite crystals.

parameter	$MAPbCl_3$	$MAPbBr_3$	$MAPbI_3$
LO phonon energy ($\hbar\omega_{\mathrm{LO}}$)	26.4 meV	15.3 meV	11.5 meV
LO phonon frequency	4.012 Hz	2.325 Hz	1.748 Hz
Effective mass (m^*)	$0.2m_0$	$0.117m_0$	$0.104m_0$

As illustrated in Fig. 2, when considering polaron velocity $u = 2\times10^4$ m/s, the variation trend of the coupling constant with the deformation potential coefficient and sound velocity of polarons in three different halide perovskite materials is illustrated. The coupling constants of materials with respective lattice constants of $a = 1$, 2, 3 exhibited common

dependencies on lattice parameters. That is, they increased with the increase of the polaron deformation potential coefficient and decreased with the increase of the sound velocity. This was because the deformation potential effect was incorporated into the total polaron system. As witnessed for deep potential wells, particles required higher energies to overcome the well and keep moving. The higher deformation potential coefficients increased the deformation potential energy, creating deeper potential wells. However, slower sound velocities in materials further restricted polaron motions within the perovskite lattice. Moreover, the motion of the polarons will in turn react back upon the lattice, inducing compressions and distortions, thereby enhancing the electron–phonon interactions.

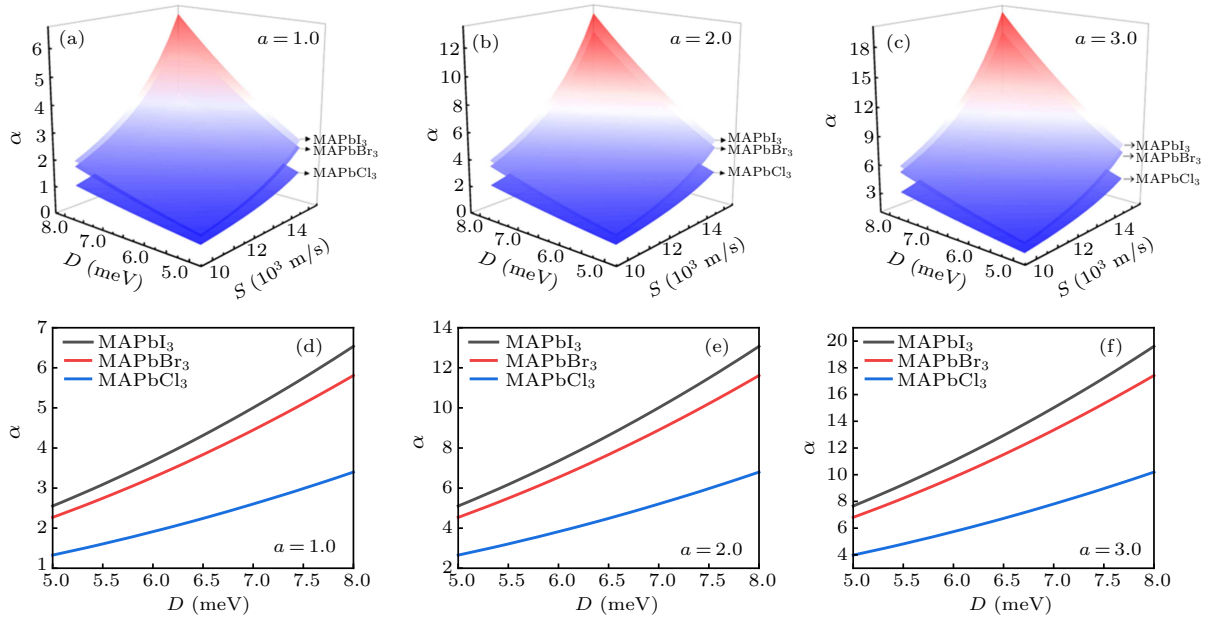


Fig. 2. The graphs (a), (b), and (c) illustrate the relationships of the coupling constant with deformation-potential constant and sound velocity. The graphs (d), (e), and (f) illustrate the relationships of the coupling constant with the deformation potential at a constant sound velocity 1×10^4 m/s.

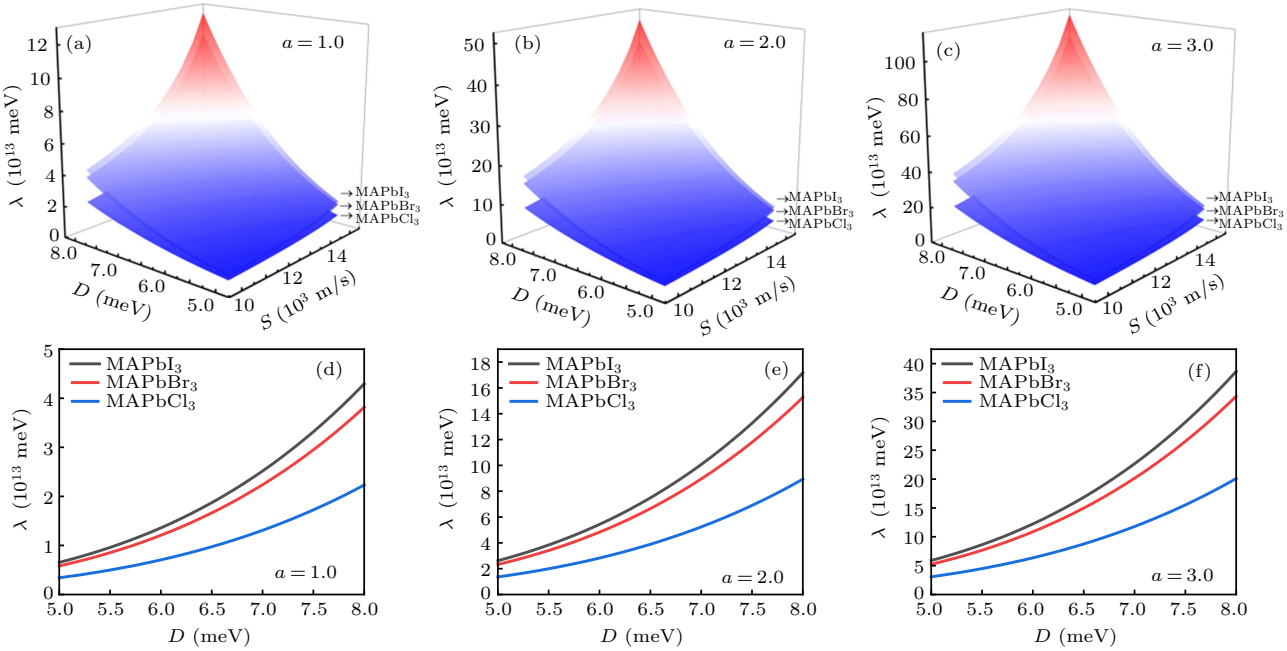


Fig. 3. The graphs (a), (b), and (c) illustrate the dependencies of vibrational frequency on deformation potential and sound velocity. The graphs (d), (e), and (f) illustrate the dependencies of vibrational frequency on deformation potential at a constant sound velocity of 1×10^4 m/s.

As a fundamental physical quantity characterizing the properties of charge carriers, vibrational frequency undergoes continuous variations influencing carrier behavior, thereby presenting unique quantum size effects of the particles. Figure 3 shows the relationship between vibrational frequency λ and both sound velocity and polaron deformation potential coefficient at polaron velocity $u = 2 \times 10^4$ m/s. As could be seen from the figure, at lattice constant values of $a = 1$, 2, 3, vi-

brational frequency was rapidly increased with both sound velocity and polaron deformation potential. This phenomenon occurred because, within the total polaron system under deformation potential effect, the polaron required additional energy to overcome the potential barrier formed by deformation potential and continue its motion. In addition, the potential barrier became deeper with the increase of deformation potential coefficient. At the same time, when considering coupling effect with acoustic phonons in the material, lattice vibrations were induced increasing the sound velocity of the material. This increased coupling caused stronger polaron vibrations, giving rise to higher vibrational frequencies.

Figure 4 illustrates the dependencies of ground-state energy E_0 on polaron deformation potential and polaron sound velocity at a polaron velocity of $u = 2 \times 10^4$ m/s. It can be seen from the figure that, for fixed lattice constants of $a = 1$, 2, 3, the ground-state energy rapidly increases with the increase of sound velocity and deformation potential. This is because larger deformation-potential coefficients create deeper potential wells, and the polaron requires more energy to keep moving. Furthermore, coupling with acoustic phonons excites lattice vibrations, raising the sound velocity of the material; *i.e.*, the increase of the intensity of vibrational frequency increases the polaron ground-state energy.

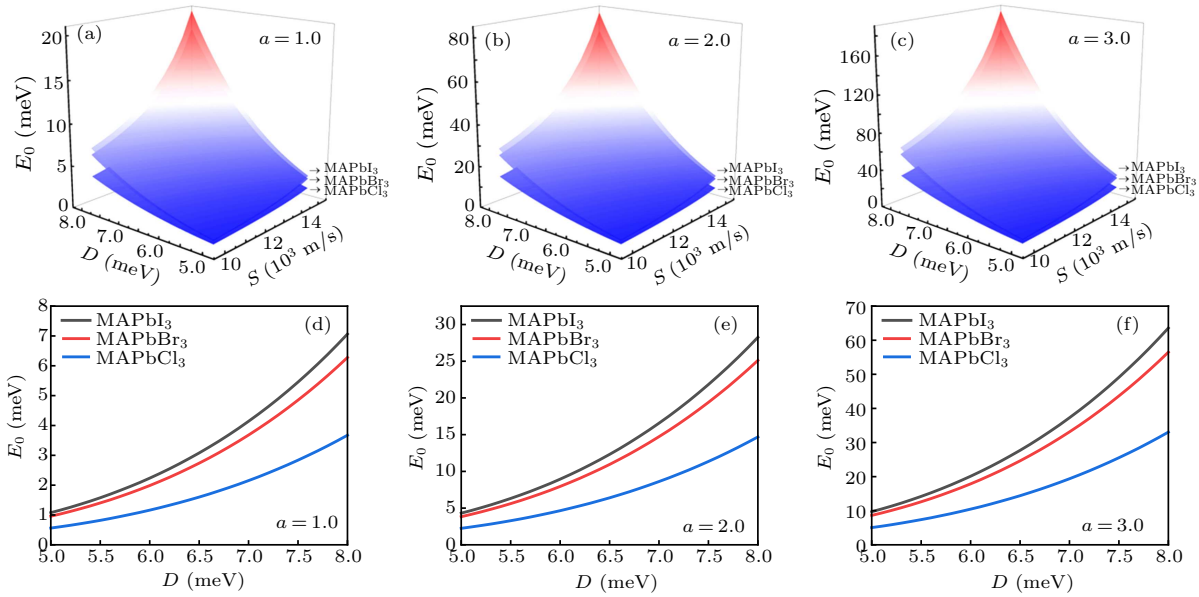


Fig. 4. The graphs (a), (b), and (c) illustrate the dependencies of ground-state energy on deformation potential and the sound velocity. The graphs (d), (e), and (f) illustrate the dependencies of ground-state energy on deformation potential at a constant sound velocity 1×10^4 m/s.

Figure 5 shows the dependencies of the effective mass m^* on polaron sound velocity and polaron deformation potential at a polaron velocity of $u = 0.8 \times 10^4$ m/s. It is evident from the figure that, for fixed lattice constant values of $a = 1$, 2, 3, the effective mass increases with the increase of the deformation-potential coefficient and decreases with the increase of sound velocity. This is because the deformation potential creates a potential well hindering polaron motion, such that an increase in well depth and a decrease in sound velocity result in a greater polaron effective mass.

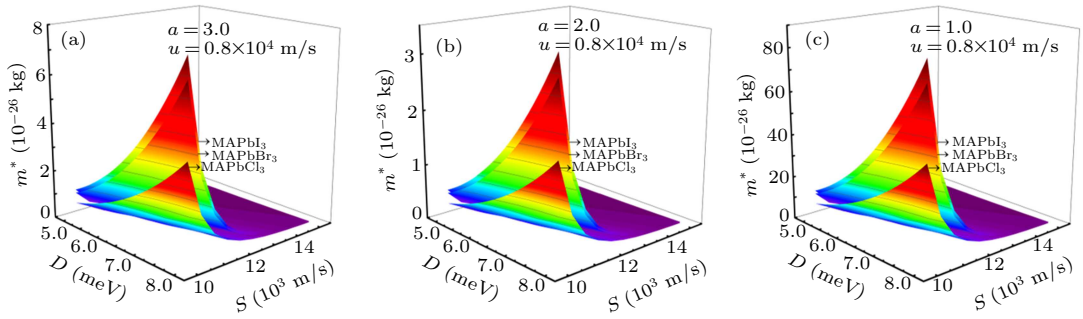


Fig. 5. The dependencies of effective mass on deformation-potential constant and sound velocity.

The profound influence of the deformation potential on the polaronic structure stems from its intrinsic mechanism of modulating the lattice potential landscape. This modulation significantly enhances the electron–phonon coupling and alters the self-trapping energy. This enhancement not only increases the effective mass and strengthens the localization of the polaron but also, via the nonlinear response of the lattice, establishes a dynamic positive feedback mechanism that ulti-

mately stabilizes this quasiparticle state. This physical picture deeply reveals the microscopic process through which external fields (stress/electric field) achieve topological control of the polaron's quantum state via the deformation potential,[31–36] providing a key theoretical basis for elucidating the mechano-electric coupling mechanism in perovskite materials.

4. Conclusions

This research investigated strongly coupled bound polaron ground-state properties in deformation potential systems using linear combination and unitary transformation operator methods. By examining polarons confined by the deformation potential, we systematically modulated the coupling constant of the material to control polaron ground-state energy and vibrational frequency, thereby enabling the evaluation of polaron effective mass for parameter-dependent property tuning. Through numerical simulations, we revealed distinct variation trends in the ground-state energy, coupling constant, effective mass, and vibrational frequency of the polaron under the effect of sound velocity and deformation potential. These findings provide crucial theoretical support to understand piezoelectric properties in perovskite materials and offer fundamental insights for experimental research on polaron effects.

Acknowledgements

Project supported by the National Natural Science Foundation of China (Grant Nos. 12164032 and 12364010), the Natural Science Foundation of Inner Mongolia Autonomous Region, China (Grant No. 2022MS01014), the Doctor Research Start-up Fund of Inner Mongolia Minzu University (Grant No. BS625), and the Basic Research Funds for Universities Directly Inner Mongolia Autonomous Region, China (Grant No. GXKY23Z029).

References

[1] Scazza F, Zaccanti M, Massignan P, Parish M M and Levinsen J 2022 *Atoms* **10** 55
[2] Pini M, Pieri P and Calvanese Strinati G 2023 *Phys. Rev. B* **107** 54505
[3] Chowdhury D, Georges A, Parcollet O and Sachdev S 2022 *Rev. Mod. Phys.* **94** 035004
[4] Shaginyan V R, Msezane A Z and Artamonov S A 2023 *Magnetism* **3** 180
[5] Yang J P, Bussolotti F, Kera S and Ueno N 2017 *J. Phys. D: Appl. Phys.* **50** 423002
[6] Bussolotti F, Yang J, Yamaguchi T, Yonezawa K, Sato K, Matsunami M, Tanaka K, Nakayama Y, Ishii H, Ueno N and Kera S 2017 *Nat. Commun.* **8** 173
[7] Malozovsky Y M and Fan J D 2010 *J. Supercond. Novel Magn.* **23** 693
[8] Zhang W, Poon T F, Tsang C W, Wang W, Liu X, Xie J, Lam S T, Wang S, Lai K T, Pourret A, Seyfarth G, Knebel G, Yu W C and Goh S K 2024 *Proc. Natl. Acad. Sci.* **121** e2322270121
[9] Berhe T A, Ashebir E K, Su W N and Hwang B J 2025 *Energy Adv.* **4** 469
[10] Benlagra A, Pruschke T and Vojta M 2011 *Phys. Rev. B* **84** 195141
[11] Zheng K, Abdellah M, Zhu Q, Kong Q, Jennings G, Kurtz C A, Messing M E, Niu Y, Gosztola D J, Al-Marri M J, Zhang X, Pullerits T and Canton S E 2016 *J. Phys. Chem. Lett.* **7** 4535
[12] Bostwick A, Ohta T, Seyller T, Horn K and Rotenberg E 2007 *Nat. Phys.* **3** 36
[13] Giustino F 2017 *Rev. Mod. Phys.* **89** 15003
[14] Falter C 2005 *Phys. Status Solidi (b)* **242** 78
[15] Setvin M, Franchini C, Hao X, Schmid M, Janotti A, Kaltak M, Walle C V de, Kresse G and Diebold U 2014 *Phys. Rev. Lett.* **113** 86402
[16] Yang S, Brant A T, Giles N C and Halliburton L E 2013 *Phys. Rev. B* **87** 125201
[17] Chen C, Avila J, Frantzeskakis E, Levy A and Asensio M C 2015 *Nat. Commun.* **6** 8585
[18] Kolesov G, Kolesov B A and Kaxiras E 2017 *Phys. Rev. B* **96** 195165
[19] Tanner A J, Wen B, Zhang Y, Liu L M, Fielding H H, Selloni A and Thornton G 2021 *Phys. Rev. B* **103** L121402
[20] Guzelturk B, Winkler T, Van De Goor T W J, Smith M D, Bourelle S A, Feldmann S, Trigo M, Teitelbaum S W, Steinrück H G, De La Pena G A, Alonso-Mori R, Zhu D, Sato T, Karunadasa H I, Toney M F, Deschler F and Lindenberg A M 2021 *Nat. Mater.* **20** 618
[21] Berger P, Attal Y, Schwarz M, Molin S, Louchet-Chauvet A, Chaneliere T, Gouet J L, Dolfi D and Morvan L 2016 *J. Lightwave Technol.* **34** 4658
[22] Tang C S, Zeng S, Wu J, Chen S, Naradipa M A, Song D, Milošević M V, Yang P, Diao C, Zhou J, Pennycook S J, Breese M B H, Cai C, Venkatesan T, Ariando A, Yang M, Wee A T S and Yin X 2023 *Appl. Phys. Rev.* **10** 031406
[23] Ding R, Zhang X and Sun X W 2017 *Adv. Funct. Mater.* **27** 1702207
[24] Chaiyo N, Cann D P and Vittayakorn N 2015 *J. Mater. Sci.* **50** 6171
[25] Kim Y J, Dang T V, Choi H J, Park B J, Eom J H, Song H A, Seol D, Kim Y, Shin S H, Nah J and Yoon S G 2016 *J. Mater. Chem. a* **4** 756
[26] Zuo R and Fu J 2011 *J. Am. Ceram. Soc.* **94** 1467
[27] Padha B, Verma S and Arya S 2022 *Adv. Mater. Technol.* **7** 2200079
[28] Deluca M and Pezzotti G 2008 *J. Phys. Chem. A* **112** 11165
[29] Sio W H and Giustino F 2023 *Nat. Phys.* **19** 629
[30] Park M, Neukirch A J, Reyes-Lillo S E, Lai M, Ellis S R, Dietze D, Neaton J B, Yang P, Tretiak S and Mathies R A 2018 *Nat. Commun.* **9** 2525
[31] Bao D, Chang Q, Chen B, Chen X, Sun H, Lam Y M, Zhao D, Zhu J X and Chia E E M 2023 *Prx Energy* **2** 13001
[32] Huang Y, Gong S, Chen Q, Chen C, Yang Z, Wang K, Xue J, Wang D, Lu H, Mao L, Yang Y, Zhao J Z and Chen X 2025 *Natl. Sci. Rev.* **12** nwae461
[33] Meggiolaro D, Ambrosio F, Mosconi E, Mahata A and De Angelis F 2020 *Adv. Energy Mater.* **10** 1902748
[34] Guo Y, Zou B, Yang F, Zheng X, Peng H and Wang J 2021 *Phys. Chem. Chem. Phys.* **23** 10153
[35] Mahata A, Mosconi E, Meggiolaro D, Fantacci S and De Angelis F 2025 *Adv. Energy Mater.* **15** 2303405
[36] Lin T, Gao A, Tang Z X, Lin W G, Sun M H, Zhang QH, Wang X F, Guo E J and Gu L 2024 *Chin. Phys. Lett.* **41** 47701